[32]R. Steele and E. Trefftz, J. Quant. Spectry. Radiative Transfer 6, 833 (1966).
[33]C. Froese, Astrophys. J. 140, 361 (1964).
[34]V. K. Prokof'ev, Z. Physik 58, 255 (1929).
[35]J. C. Stewart and M. Rotenberg, Phys. Rev. 140, A1508 (1965).
[36]A. W. Weiss, to be published.
[37]A. S. Douglas and R. H. Garstang, Proc. Cambridge Phil. Soc. 58, 377 (1962).
[38]C. E. Moore, Atomic Energy Levels, Natl. Bur. Std. (U. S.), Circ. No. 467 (U. S. Government Printing Office, Washington, D. C., 1949), Vol I.
[39]C. E. Moore, Selected Tables of Atomic Spectra, Natl. Stand. Ref. Data Series-NBS 3, Sec. 1 (U. S. Government Printing Office, Washington, D.C., 1965).
[40]C. W. Allen, Monthly Notices Roy. Astron. Soc. 121, 299 (1960).
[41]Our numbers are based on the critically evaluated data of Ref. 8.
[42]E. M. Anderson and V. A. Zilitis, Opt. i Spektroskopiya 16, 177 (1964) [English transl.: Opt. Spectry. (USSR) 16, 99 (1964)]
[43]A. Fillipov and V. K. Prokof'ev, Z. Physik 56, 458 (1929).
[44]A. N. Fillipov, Z. Physik 69, 526 (1931).
[45]For the first few lines of this series, additional theoretical data are available, which give the same qualitative behavior.
[46]G. Jürgens, Z. Physik 138, 613 (1954).
[47]J. E. Solarski and W. L. Wiese, Phys. Rev. 135, A1236 (1964).
[48]E. W. Foster, Proc. Phys. Soc. (London) A79, 94 (1962).

PHYSICAL REVIEW VOLUME 175, NUMBER 1 5 NOVEMBER 1968

Spins and Nuclear Moments of Sb^{115}, Sb^{117}, Sb^{118}, Sb^{119}, and Sb^{120}†

A. D. Jackson, Jr.,* E. H. Rogers, Jr.,‡ and G. J. Garrett§
Palmer Physical Laboratory, Princeton University, Princeton, New Jersey
(Received 19 July 1968)

We have measured the spins and hyperfine structures of several antimony isotopes by atomic-beam magnetic-resonance methods. The isotopes were produced by proton bombardment of isotopically-enriched tin in the Princeton cyclotron. The experiments gave the following results:

Isotope		I	a (MHz)	b (MHz)	μ_I (μ_N) (diamagnetically corrected)	Q(b)
Sb^{115}	(31 min)	5/2	-307.68(19)	-3.7(5)	+3.46(1)	-0.20(4)
Sb^{117}	(2.8 h)	5/2	-237.91(15)	-5.5(5)	+2.67(1)	-0.30(5)
Sb^{118}	(3.5min)	1	±547(13)	...	±2.46(7)	...
Sb^{119}	(38 h)	5/2	-307.16(6)	-3.8(4)	+3.45(1)	-0.21(4)
Sb^{120}	(16min)	1	±520(47)	...	±2.34(22)	...

The experiment on Sb^{119} gives g_J(Sb) = -1.970 60(6). The magnetic moments of these and other antimony isotopes are discussed in terms of configuration-mixing calculations using matrix elements of the Hamada-Johnston potential.

1. INTRODUCTION

Theoretical investigations of nuclear structure have been particularly rewarding in regions of the periodic table where properties are known for a large number of related nuclei. In such cases it is often possible to explain the data with a relatively small number of parameters which are taken from theory or from best fits to experimental data. In view of the overdetermination of these parameters, the quality of the agreement between experiment and theory can be a useful measure of the validity of the nuclear model under consideration. The numerous isotopes of the element antimony provided an opportunity for work along these lines. There are two stable antimony isotopes and 32

radioactive species, including ground states and isomers with half-lives longer than 20 seconds. Spins and magnetic moments had been measured for five of these 34 states, as well as for the first excited state of Sb^{121}, previous to the present experiments. 12 of the remaining states can be produced by (p,n) or $(p,2n)$ reactions on stable tin isotopes. These antimony isotopes are well suited for study by atomic-beam methods because of their half-lives. Since the corresponding stable tin isotopes are readily available in high-isotopic enrichment, it was considered worthwhile to find techniques for obtaining atomic beams of antimony from tin targets. The beam-production techniques developed in the initial experiments on Sb^{117} were used with only minor changes for the work on other antimony isotopes.

The large number of stable tin isotopes is indicative of the proton-shell closure at $Z=50$. The magnetic moments of the antimony isotopes are of considerable theoretical interest, as a simple interpretation of the data may be expected to yield satisfactory results for configurations near closed shells. Section 4 presents the results of a first-order configuration-mixing calculation of the antimony magnetic moments using techniques introduced by Blin-Stoyle[1] and Noya, Arima, and Horie[2].

For a description of the theory of hyperfine structure relevant to these measurements, the reader is referred to books by Ramsey[3] and Kopfermann.[4]

2. EXPERIMENTAL DETAILS

A. Beam Apparatus

The hyperfine structure (hfs) measurements were made with standard atomic-beam magnetic-resonance methods. The work on Sb^{118} and Sb^{120} involved the atomic-beam apparatus which is on line with the external proton beam of the Princeton cyclotron; an off-line apparatus was used for Sb^{115}, Sb^{117}, and Sb^{119}. The magnet systems of the two machines are identical in their essential details. A six-pole A magnet transmits only atoms with atomic spin projection $m_J>0$. Radio-frequency (rf) transitions are induced among the hfs states as the atoms pass through a homogeneous two-pole C magnet, and an inhomogeneous two-pole B magnet then separates the "flopped" atoms (which have undergone a transition $m_J>0 \rightarrow m_J<0$) from the "beam" atoms (which have $m_J>0$). The flop and beam atoms are deposited on a pair of etched iron collectors, which are inserted into the apparatus through an airlock. The hfs resonances are observed by counting the relative number (F/B) of atoms in the flop and beam as a function of the frequency of the oscillating magnetic field which induces the transitions. Further details regarding the equipment are given elsewhere.[5,6]

B. Beam Production and Detection

The 31-min Sb^{115}, 2.8-h Sb^{117}, and 38-h Sb^{119} were produced in the internal cyclotron beam by the reactions $Sn^{116}(p,2n)Sb^{115}$, $Sn^{117}(p,n)Sb^{117}$, and $Sn^{119}(p,n)Sb^{119}$.[7] The proton current was limited to 1.5 μA to avoid melting the tin, which was wrapped in 2-mil aluminum foil to contain the tin in the event that melting occurred. The 20-mil-thick Sn^{117} and Sn^{119} targets were bombarded with 17.5-MeV protons. The proton energy was increased to 18.5 MeV for the Sn^{116} bombardments in order to increase the $(p,2n)$ yield. A reduced target thickness (12 mil) was used for the Sn^{116} to optimize the $(p,2n)$ yield relative to the (p,n) yield by discarding protons with energies lower than the Q-value of the $(p,2n)$ reaction. Following the proton bombardment, the activated targets were allowed to decay before the start of atomic-beam work to reduce the effects of short-lived contaminants (see below) and also for the convenience (in the case of Sb^{119}) of carrying out the atomic-beam run on the day after the proton irradiation. The bombardment and decay periods for Sb^{115} were 1 h and $\frac{1}{2}$ h, respectively; for Sb^{117}, 3 h and 2 h; for Sb^{119}, 4 h and 18 h.

After the decay period, the target was transferred to an atomic beam oven, which was inserted into the apparatus through an airlock. The oven used for Sb^{115}, Sb^{117}, and Sb^{119} is shown in Fig. 1. The inner oven of boron nitride served to reduce fluctuations in the atomic-beam intensity. Early runs with a plain molybdenum oven showed that the melted tin, which wets molybdenum, crept forward to clog the oven hole, causing erratic beam behavior and finally cutting off the beam entirely. Tin does not wet boron nitride, and the tin showed no tendency to creep inside the BN liner. It was then possible to obtain stable behavior in the antimony beam over the course of a run. When the activity was exhausted, the tin target was readily removed for re-use, as the tin forms a ball which does not adhere to the BN liner. The Sn^{117} and Sn^{119} targets lost about 3 mg per run from an oven load of 150 mg. The Sn^{116} targets, which were heated to higher temperatures, lost 5–10 mg per run.

Electron bombardment was used to heat the oven, whose temperature was measured with an optical pyrometer. The oven was operated at 1175°C for Sb^{117} and 1225°C for Sb^{119}. The temperatures given here are the uncorrected optical pyrometer readings on the oven jacket. Because of the short half-life of Sb^{115}, it was necessary to gradually increase the oven temperature from 1225°C to 1275°C over the course of each Sb^{115} run in order to keep the counting statistics uniform for all data points. The collection and counting times were also increased over the course of each Sb^{115} run for the

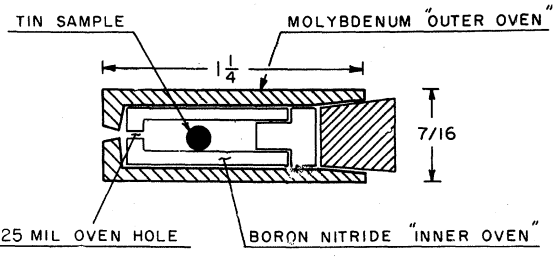

FIG. 1. Boron nitride oven and molybdenum jacket used for long-lived antimony isotopes. (Dimensions are given in inches.)

same reason. The Sb^{115} collection time was varied from 2 to 10 min, and the collected activity was counted from 5 to 30 min. For a 4-min collection and a 10-min count, the Sb^{115} beam collectors gave around 12 000 counts. The collection time for each Sb^{117} datum point was 15 min; each collector was counted for a total of about 60 min, giving 500 to 1000 counts on the beam collectors. For Sb^{119} the collection time was 15 min, and the counting period was 2 h for each flop collector and 1 h for each beam collector. A typical beam collector gave 6000 counts.

The 3.5-min Sb^{118} and 16-min Sb^{120} were produced by the reactions $Sn^{118}(p,n)Sb^{118}$ and $Sn^{120}(p,n)Sb^{120}$ in the oven chamber of the on-line atomic beam apparatus. A 300-mg sample of the appropriate tin isotope was placed in the inner oven of boron nitride (see Fig. 2). The heated oven was bombarded with a 0.25–0.35 μA beam of 17.5-MeV protons, which reached the tin target through a slot in the molybdenum jacket and a 5-mil-thick section in the wall of the BN oven. The oven was heated to 1225°C by electron bombardment. The collection and counting times for Sb^{118} were 8 min and 6 min, respectively, with a turnaround time of about 90 sec between the end of a collection and the start of counting. (Similar turnaround times elapsed in all the counting procedures, but only for this isotope was the time a significant fraction of the half-life.) The collection and counting periods for Sb^{120} were both 10 min. The beam collectors for Sb^{118} and Sb^{120} gave from several hundred up to several thousand counts. The sizable variation of atomic-beam intensity in the work with the on-line apparatus was attributed in part to drifts in the proton-beam intensity. Instabilities in the behavior of the atomic beam were reduced somewhat by turning off the proton beam only during the few seconds when access to the apparatus was necessary.

Four of the experimental isotopes ($Sb^{115,117,118,120}$) emit positrons or electrons of appreciable energy in a significant fraction of their decays, so that the flop and beam activity in these experiments could be detected efficiently with 1/16-in.-thick plastic scintillators. The strong β^+ emitters are Sb^{115} (36%, 1.51 MeV), Sb^{118} (81%, 3.10 MeV; 2%, 1.88 MeV), and Sb^{120} (44%, 1.70 MeV). The decay of Sb^{117} goes almost entirely (97.5%) by electron capture to the 161-keV level in Sn^{117}. This state decays by an M1 transition which produces a 133-keV conversion electron in 10% of the cases.[8]

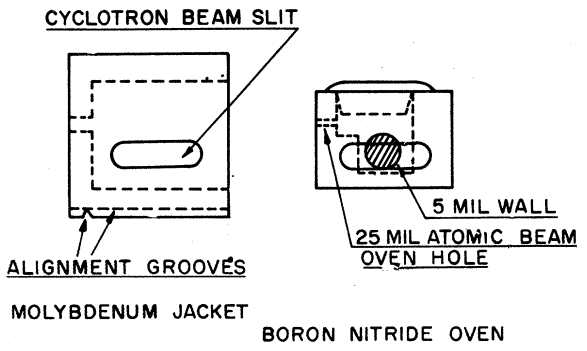

FIG. 2. Boron nitride oven and molybdenum jacket used for short-lived antimony isotopes.

The ground state of Sb^{119} decays entirely by electron capture to the 24-keV level in Sn^{119}. The conversion electrons resulting from the decay of this state in Sn^{119} have insufficient energy to penetrate the collector-mounting tape and the two layers of 1/4-mil aluminum foil which were used for shielding the plastic scintillators from light. The activity collected from the Sb^{119} beam was thus detected by counting the 24-keV γ-decays in Sn^{119} with 1-mm-thick NaI(Tl) scintillators.

The detectors were surrounded with an inner shield of iron and an outer shield of lead. Discriminators were set to eliminate low-energy noise counts. The background counting rate was about three counts per min for the plastic scintillators and six counts per min for the NaI(Tl) scintillators.

The chief contaminant of the 31-min Sb^{115} was 15.5-min Sb^{116}, which was produced by the reaction $Sn^{116}(p,n)Sb^{116}$. A small amount of 1-h Sb^{116m} was also produced. These isotopes were identified in an irradiated target from a γ-ray spectrum taken with a Ge(Li) detector. The ratio of Sb^{115} activity to the total activity was determined as a function of the time after bombardment by obtaining a decay curve of the total activity using the same plastic scintillators as for the atomic-beam work. This result was used to maximize the hfs resonance signals by counting the atomic-beam activity in the period during which Sb^{115} comprised more than 60% of the total activity. A half-life measurement for the activity on a flop collector demonstrated that the observed hfs resonances were due to Sb^{115}. Further evidence for this was the fact that the resonance frequencies indicated a half-integral spin ($I = 5/2$); Sb^{115} was the only odd-A nucleus present in significant amounts.

The presence of Sb^{117} as the major activity in an irradiated Sn^{117} target was verified from a γ-ray spectrum taken with an NaI(Tl) detector. Owing to the lower isotopic purity of the Sn^{117} sample (see Table I), it was expected that the Sb^{117} beam might contain appreciable contamination from 15.5-min Sb^{116}, 3.5-min Sb^{118}, 16-min Sb^{120}, 1-h Sb^{116m}, 5.1-h Sb^{118m}, and 38-h Sb^{119}. The 2-h waiting

TABLE I. Isotopic analysis of tin targets, reported by Oak Ridge National Laboratory, which supplied the tin samples. Several of the observed constituents with abundances of less than 0.3% are not shown. The isotopic purity of the Sn^{118} sample was 98.6%.

Stable isotope	Sn^{116} target	Sn^{117} target	Sn^{119} target	Sn^{120} target
116	95.74	2.57	0.65	0.2
117	1.02	78.8	0.63	0.12
118	1.49	8.03	3.01	0.5
119	0.32	7.19	89.8	0.39
120	1.06	2.84	5.34	98.39

period between the proton bombardment and the atomic beam experiment served to reduce the contributions of short-lived contaminants to negligible levels. A decay curve of the activity on a beam collector showed no significant counting of contaminants.

The Sb^{119} beam was expected to be free of contamination because of the high enrichment of the Sn^{119} target. A γ-ray spectrum of an activated Sn^{119} target demonstrated high purity for the resulting Sb^{119} activity. The short-lived Sb^{118} and Sb^{120} (produced from the small Sn^{118} and Sn^{120} impurities) were eliminated by the 18-h wait before the atomic beam run. A decay curve of the activity on a flop collector showed that the hfs resonances were due to Sb^{119}.

The purity of the Sn^{118} and Sn^{120} samples was also very high, so that no significant contamination was expected for the corresponding antimony isotopes. The atomic beams were identified as Sb^{118} and Sb^{120} from half-life measurements on activity collected from the beams.

3. RESULTS

The hfs transtiions involved in these measurements are shown in Figs. 3 and 4. The data are summarized in Tables II-VI, and sample experimental resonances are shown in Figs. 5–9. The

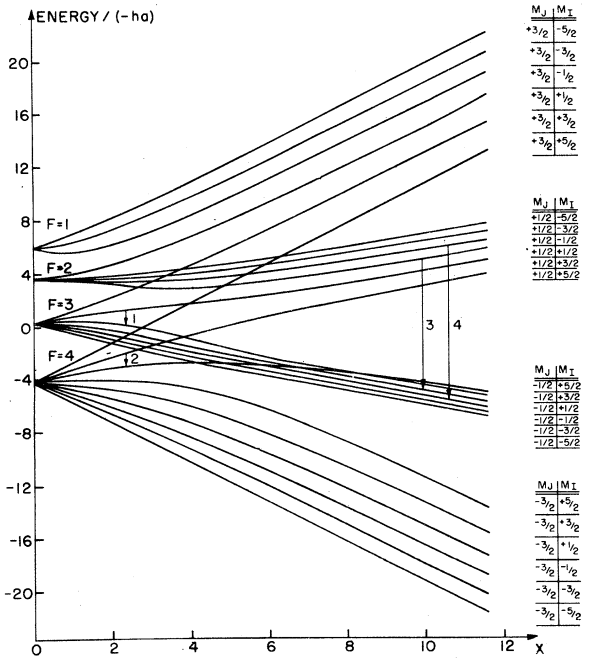

FIG. 3. Hyperfine-structure energies for Sb^{115}, Sb^{117}, and Sb^{119} ($I=5/2$, $J=3/2$, $a<0$, $\mu_I>0$). The magnetic field H_C is plotted in terms of the dimensionless parameter $x=\mu_0 g_J H_C/ha$. Transitions observed in this work are designated by arrows. The direct transitions 3 and 4 are drawn in the high-field region for clarity; observations on these transitions were made at low fields. Transition 1 involves $(F,M)=(3,2)\rightarrow(3,1)$; transition 2, $(4,3)\rightarrow(4,2)$; transition 3, $(2,1)\rightarrow(3,0)$; transition 4, $(2,0)\rightarrow(3,-1)$.

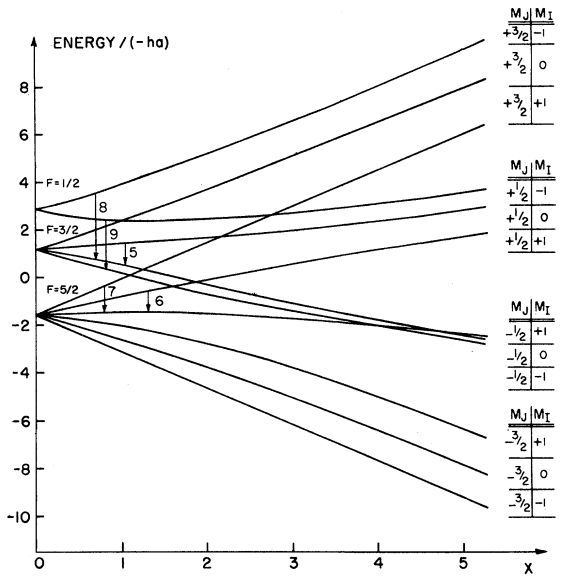

FIG. 4. Hyperfine-structure energies for Sb^{118} and Sb^{120} ($I=1$, $J=3/2$; it is assumed that $a<0$, and hence $\mu_I>0$). The magnetic field H_C is plotted in terms of $x=\mu_0 g_J H_C/ha$. Transitions observed in this work are designated by arrows. Transition 5 involves $(F,M)=(3/2,1/2)\rightarrow(3/2,-1/2)$; transition 6, $(5/2,3/2)\rightarrow(5/2,1/2)$; transition 7, $(5/2,5/2)\rightarrow(5/2,1/2)$; transition 8, $(1/2,1/2)\rightarrow(3/2,-1/2)$; transition 9, $(1/2,-1/2)\rightarrow(3/2,-3/2)$.

TABLE II. Summary of hfs data for Sb^{115}, as reduced by HYPERFINE-4A (see Ref. 9). Results of least-squares fit: $a=-307.68(19)$ MHz, $b=-3.7(5)$ MHz; $\chi^2=1.8$. Comparison isotope (see text): Sb^{121}, $^4S_{3/2}$, $I=5/2$, $g_J=-1.970\,06(6)$, $\mu_I=3.3416\mu_N$ (diamagnetically uncorrected), $a=-299.034$ MHz, $b=-3.68(2)$ MHz, $Q=-0.20(3)\,b$. Calibration isotope: K^{39}, $^2S_{1/2}$, $g_J=-2.002\,295\,1\,(22)$, [a] $\mu_I=0.390\,97\,(15)\mu_N$ (diamagnetically uncorrected), [b] $a=230.859\,845(15)$ MHz. [c] These comparison and calibration data apply for Tables II—VI.

K^{39} calibration frequency (MHz)	Sb^{115} frequency (MHz)	Resonance assignment (see Fig. 3)	Residual and probable error (kHz)
4.8845(15)	7.033(4)	2	-2(5)
10.2220(10)	14.361(3)	2	-4(3)
20.1865(15)	27.138(4)	2	-2(4)
41.9795(15)	51.940(5)	2	0(5)
41.9755(35)	42.828(7)	1	-2(8)
99.8490(30)	105.122(4)	2	0(5)
99.8650(40)	91.058(4)	1	0(5)

[a] K. D. Böklen, W. Dankwort, E. Pitz, and S. Penselin, Z. Physik 200, 467 (1967).

[b] J. T. Eisinger, B. Bederson, and B. T. Feld, Phys. Rev. 86, 73 (1952).

[c] A. L. Bloom and J. B. Carr, Phys. Rev. 119, 1946 (1960).

TABLE III. Summary of hfs data for Sb^{117}. Result of least-squares fit: $a=-237.91(15)$ MHz, $b=-5.5(5)$ MHz; $\chi^2=5.8$. (See also caption for Table II.)

K^{39} calibration frequency (MHz)	Sb^{117} frequency (MHz)	Resonance assignment (see Fig. 3)	Residual and probable error (kHz)
5.135(5)	7.404(5)	2	+1(9)
6.816(2)	9.751(10)	2	-3(10)
8.982(2)	12.733(4)	2	-1(5)
8.978(2)	12.735(4)	2	+6(5)
19.464(5)	26.422(7)	2	-15(9)
19.472(3)	26.447(5)	2	0(6)
34.899(19)	44.820(2)	2	+14(22)
36.064(6)	46.110(5)	2	-9(8)
95.115(2)	103.748(6)	2	+1(6)
94.861(4)	92.090(10)	1	0(11)

strength of the transition-inducing rf field needed to maximize the heights of one-quantum antimony resonances was calculated from measurements of optimum rf powers for resonances in stable K^{39}. Resonances were produced using the predicted rf field strengths for all ranges of the static magnetic field H_C; this served to identify these peaks as one-quantum transitions. Both of the observable one-quantum transitions (1 and 2 in Fig. 3; 5 and 6 in Fig. 4) were seen for each isotope. Higher rf powers were used to locate the two-quantum resonance 7 in Sb^{118} and Sb^{120}. The peaks were found at the expected frequencies, giving additional evidence for the transition assignments for these isotopes (Tables IV and VI). The $\Delta F=1$ transitions 8 and 9 were observed in Sb^{118}; they were identified by their frequency separation. Resonances were obtained for the $\Delta F=1$ transitions 3 and 4 in Sb^{119} (see Fig. 3). These resonances were observed at $H_C=0.978(7)$ G; their identification is based on the observation of 4 at several other fields (Table V).

Observation of $\Delta F=0$ transitions at low fields H_C served to establish the values of the nuclear spins:

TABLE IV. Summary of hfs data for Sb^{118}. Result of least-squares fit assuming $a<0$: $a=-538(1)$ MHz, $b=+3.3(8)$ MHz; $\chi^2=6.7$. (See also caption for Table II.)

K^{39} calibration frequency (MHz)	Sb^{118} frequency (MHz)	Resonance assignment (see Fig. 4)	Residual and probable error (kHz)
6.607(7)	15.030(15)	6	+6(21)
12.709(2)	28.075(10)	7	+9(11)
18.562(4)	39.670(20)	6	+5(21)
29.899(3)	60.595(25)	6	-14(26)
33.542(3)	66.937(6)	6	+11(8)
33.542(2)	66.930(5)	6	+4(6)
54.406(4)	100.020(10)	6	-18(12)
54.293(11)	122.220(10)	5	+8(23)
0.804(11)	818.580(80)	8	-52(95)
0.804(11)	815.700(50)	9	+15(51)

TABLE V. Summary of hfs data for Sb^{119}. Result of least-squares fit: $a=-307.16(6)$ MHz, $b=-3.8(4)$ MHz, $g_J=-1.97060(6)$; $\chi^2=1.7$. (See also caption for Table II.)

K^{39} calibration frequency (MHz)	Sb^{119} frequency (MHz)	Resonance assignment (see Fig. 3)	Residual and probable error (kHz)
5.276(2)	7.588(5)	2	+3(6)
7.884(2)	11.196(7)	2	+1(8)
12.644(2)	17.568(4)	2	+3(5)
20.338(2)	27.326(4)	2	-1(5)
30.569(2)	39.430(15)	2	+2(15)
30.561(3)	32.098(4)	1	-2(5)
54.925(2)	65.131(3)	2	+2(4)
54.913(3)	54.395(3)	1	0(4)
100.281(5)	105.487(4)	2	-3(6)
100.278(5)	91.408(5)	1	-1(6)
0.688(5)	919.990(25)	3	-9(25)
0.688(5)	920.550(30)	4	-8(31)
0.632(5)	920.500(10)	4	+5(11)
0.497(5)	920.340(20)	4	-1(21)
0.873(5)	920.765(10)	4	-2(11)

$I(Sb^{115})=I(Sb^{117})=I(Sb^{119})=5/2$; $I(Sb^{118})=I(Sb^{120})=1$. These results were also confirmed by the work at higher fields.

A least-squares fit of a, b, and g_J to the Sb^{119} hfs data (Table V) gives $a(Sb^{119})=-307.16(6)$ MHz, $b(Sb^{119})=-3.8(4)$ MHz, and $g_J(Sb^{119})=-1.970\,60(6)$ with $\chi^2=1.7$ or $a(Sb^{119})=+306.96(7)$ MHz, $b(Sb^{119})=+2.5(4)$ MHz, and $g_J(Sb^{119})=-1.968\,42(6)$ with $\chi^2=17$.[9] The second fit (with positive a and b values) is unacceptable, since the g_J value does not agree with the earlier value $g_J(Sb)=-1.9705(2)$.[10] We therefore conclude that the Sb^{119} data are properly represented by the first fit. The value $g_J(Sb)=g_J(Sb^{119})=-1.970\,60(6)$ was used in the analysis of all the present hfs data. Values listed for other hfs parameters include the effect of the uncertainty in $g_J(Sb)$.

Least-squares fits of a and b to the data of Tables II and III were carried out (with g_J fixed at $-1.970\,60$) for both possible signs of a. The best values (with the favored sign choices) are, in MHz,

TABLE VI. Summary of hfs data for Sb^{120}. Result of least-squares fit, assuming $a<0$: $a=-492(18)$ MHz; $\chi^2=3.4$. (See also caption for Table II.)

K^{39} calibration frequency (MHz)	Sb^{120} frequency (MHz)	Resonance assignment (see Fig. 4)	Residual and probable error (kHz)
1.547(2)	3.625(15)	6	4(16)
6.142(2)	14.025(15)	6	+17(16)
9.523(5)	21.328(18)	6	+2(21)
9.847(1)	22.010(10)	6	-3(10)
9.847(1)	22.088(10)	7	+11(10)
18.684(2)	39.920(20)	6	-19(20)

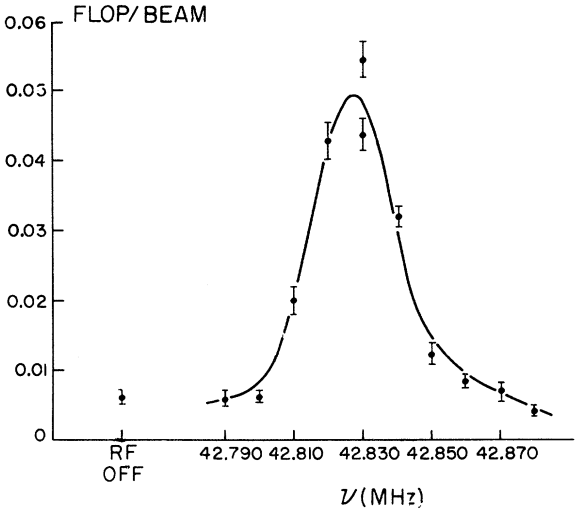

FIG. 5. Resonance 1 (see Fig. 3) in Sb^{115} at H_c = 47.935 (3) G.

$a(Sb^{115}) = -307.68(19)$, $b(Sb^{115}) = -3.7(5)$, $a(Sb^{117}) = -237.91(15)$, and $b(Sb^{117}) = -5.5(5)$. The χ^2 values corresponding to the best fits for the favored and unfavored sign choices for Sb^{115} are 1.8 and 111, respectively; for Sb^{117}, 5.8 and 43. The data thus give negative a values for these isotopes.

A least-squares fit of a to the Sb^{120} data (Table VI) gives $a(Sb^{120}) = -492(18)$ or $+545(22)$ MHz. The data show no preference for either sign, so we quote the value as $|a(Sb^{120})| = 520(47)$ MHz. The uncertainty in this value includes an additional 3 MHz to allow for the possible effect of an electric quadrupole interaction corresponding to $b = \pm 5$ MHz. (The data were not sufficiently accurate to yield a value for b, but a shell-model estimate based on empirical quadrupole moments indicates that $|b| < 5$ MHz for Sb^{118} and Sb^{120}.)

A least-squares fit of a and b to the Sb^{118} data of Table IV (with g_J fixed at $-1.970\,60$) gives $a(Sb^{118})$

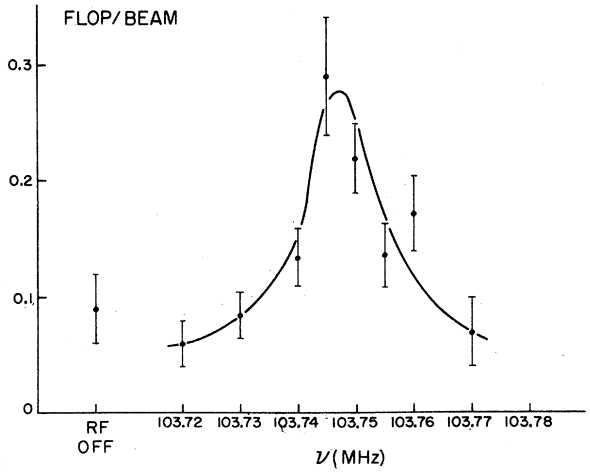

FIG. 6. Resonance 2 (see Fig. 3) in Sb^{117} at H_c = 89.763 (1) G.

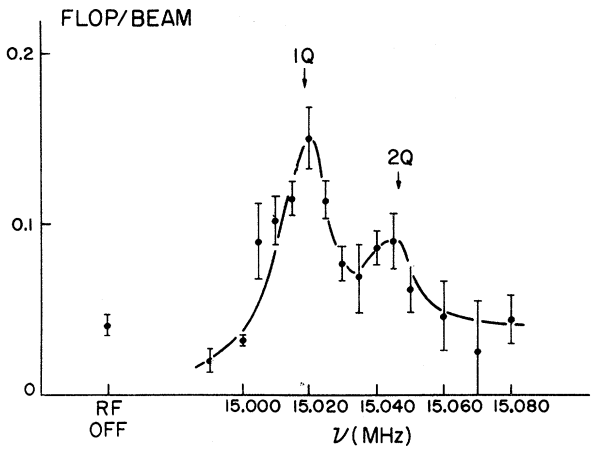

FIG. 7. The one- and two-quantum resonances 6 and 7 (see Fig. 4) in Sb^{118} at $H_c = 9.049(9)$ G.

$= -538(1)$ MHz and $b(Sb^{118}) = +3.3(8)$ MHz with $\chi^2 = 6.7$ or $a(Sb^{118}) = +556(1)$ MHz and $b(Sb^{118}) = +8.7(9)$ MHz with $\chi^2 = 7.1$. Additional observations at higher fields were inconclusive in determining the sign of a and the value of b for this isotope because of inconsistencies in the data. A fit of a, b, and g_J to all of the Sb^{118} data gives a satisfactory χ^2 value for $a > 0$, but the resulting $g_J(Sb^{118}) = -1.969\,75(6)$ disagrees badly with the old g_J value, and the Sb^{118} and Sb^{119} data cannot be fitted satisfactorily using this g_J value. The fit for $a < 0$ gives an unsatisfactorily large χ^2; the resulting $g_J(Sb^{118}) = -1.970\,36(6)$ is closer to our $g_J(Sb^{119})$, although the values still disagree. If the complete Sb^{118} data are analyzed with g_J fixed at $-1.970\,60$, the values of a and b change markedly from the values listed at the beginning of the paragraph, (the sign of b changes for the fit with $a < 0$) and the χ^2 values become unsatisfactorily large. In view of these discrepancies, we quote the result of the Sb^{118} measurements as $|a(Sb^{118})| = 547(13)$ MHz, again allowing an additional uncertainty of 3 MHz for a possible electric quadrupole interaction, as was done for Sb^{120}.

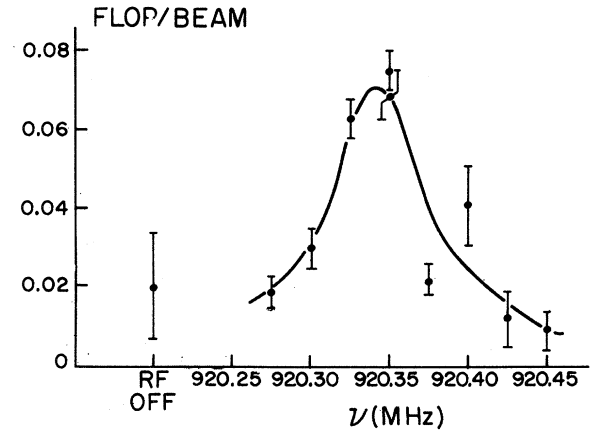

FIG. 8. The $\Delta F = 1$ resonance 4 (see Fig. 3) in Sb^{119} at $H_c = 0.682(7)$ G.

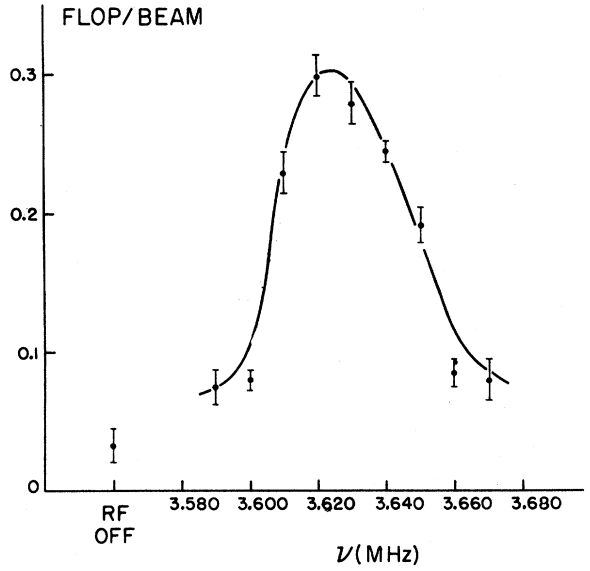

FIG. 9. Resonance 6 (see Fig. 4) in Sb^{120} at H_C = 2.187 (3) G.

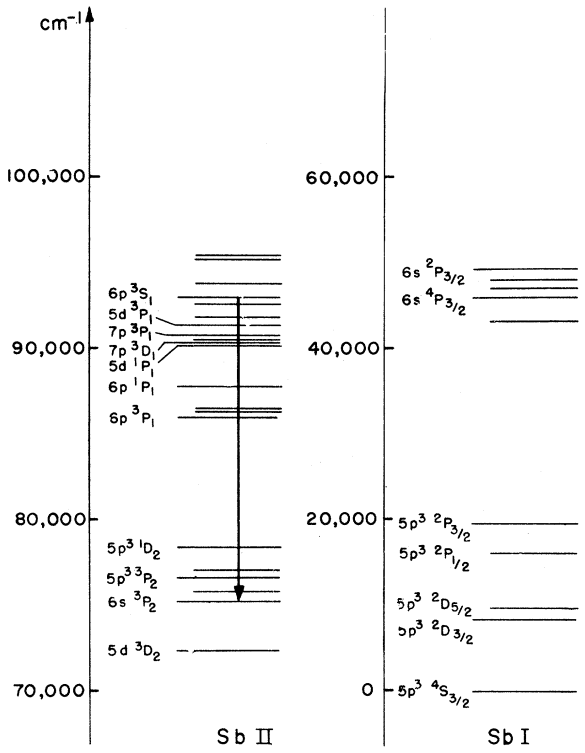

FIG. 10. Electronic energy levels for singly-ionized antimony (Sb II) and neutral antimony (Sb I), as obtained from C. E. Moore, Atomic Energy Levels, National Bureau of Standards Circ. No. 467, (U.S. Government Printing Office, Washington, D.C., 1958), Vol. III.

From our experimental a values we calculate the corresponding magnetic dipole moments using the Fermi-Segrè relation[3] with Sb^{121} as the reference isotope: $a(Sb^{121}) = -299.034(4)$ MHz,[10] $\mu_I(Sb^{121}) = +3.3590\mu_N$ (diamagnetically corrected),[11] $I(Sb^{121}) = 5/2$. The resulting values are: $\mu_I(Sb^{115}) = +3.46(1)\mu_N$, $\mu_I(Sb^{117}) = +2.67(1)\mu_N$, $|\mu_I(Sb^{118})| = 2.46(7)\mu_N$, $\mu_I(Sb^{119}) = +3.45(1)\mu_N$, and $|\mu_I(Sb^{120})| = 2.34(22)\mu_N$ (diamagnetically corrected). An uncertainty of 0.3% has been included to allow for possible hfs anomalies. (The hfs anomaly between Sb^{121} and Sb^{123} is 0.3%.[10])

In order to obtain the values of the nuclear electric quadrupole moment Q corresponding to the measured b values, we have used the theoretical antimony Q/b ratio of Fernando *et al.*,[10] believing their extraction of the Sb^{121} and Sb^{123} quadrupole moments from hfs data to be more reliable than that of Murakawa.[12] The latter study, which gives larger Q values by a factor of 2.5, is based on observations of the optical hfs of the transition between the two atomic states $5s^25p6p\ ^3S_1$ and $5s^25p6s\ ^3P_2$ in singly-ionized antimony (Sb II; see Fig. 10). The atomic electric field gradients of these states are calculated under the assumption of pure LS-coupling states for the electronic wave functions, although the LS-coupling scheme cannot be obeyed exactly because of Coulomb repulsion between the electrons and the existence of spin-orbit forces. The treatment ignores the effect of four $J=1$ levels within 3000 cm^{-1} of the initial $^3S_1$ states and three $J=2$ levels within 5000 cm^{-1} of the final $^3P_2$ state (see Fig. 10). On the other hand, Fernando *et al.* measured $b(Sb^{121})$ and $b(Sb^{123})$ in the neutral antimony ground state (Sb I) using atomic beam methods. For the calculation of the electric field gradient at the nucleus they expressed the electronic wave function of the $J=3/2$ ground state as a linear combination of the three $J=3/2$ LS-coupling states ($^4S_{3/2}$, $^2P_{3/2}$, $^2D_{3/2}$) which can be formed from the $5s^25p^3$ ground-state configuration of Sb I. The treatment thus includes the effects of all states within 45 000 cm^{-1} of the Sb I ground state (see Fig. 10). Moreover, since the operator of the electric field gradient is a one-body tensor operator of rank two, the $5s^25p7p\ ^3D_1$ level can generate a first-order correction to the field gradient of the $^3S_1$ level in Sb II. The $J=3/2$ states at 45 000 cm^{-1} in Sb I involve the promotion of a single $5p$ electron to a $6s$ orbit, so these states can generate no first-order corrections to the electric field gradient of the ground state.

Using the values $b(Sb^{121}) = -3.68(2)$ MHz and $Q(Sb^{121}) = -0.20(3)\ b$ of Fernando *et al.*, we then obtain $Q(Sb^{115}) = -0.20(4)\ b$, $Q(Sb^{117}) = -0.30(5)\ b$, and $Q(Sb^{119}) = -0.21(4)\ b$.

4. DISCUSSION

In view of the present measurements, experimental values are now known for the nuclear magnetic moments of eleven states in the antimony isotopes. This section presents a calculation of these moments in

which the antimony wave functions are obtained empirically under the initial assumption that they are of lowest possible seniority. These wave functions are used to evaluate corrections to the magnetic moment due to first-order configuration mixing. Smaller corrections due to the apparent one-body spin-orbit potential and quenching of the anomalous moment of the odd proton are also included.

A. Odd-A Magnetic Moments

Since antimony has one proton past the closed shell at $Z=50$, we describe the odd-A antimony wave functions as a single proton in either the $2d_{5/2}$ or $1g_{7/2}$ levels and a seniority-0 ensemble of neutrons in the levels $2d_{5/2}$, $1g_{7/2}$, $2d_{3/2}$, $3s_{1/2}$, and $1h_{11/2}$. (The nature of this neutron wave function will be discussed below.) The magnetic moment of such a configuration is simply the Schmidt-moment of the unpaired proton. This moment is not an adequate description of real antimony moments (see Table VII), but the wave function does provide a starting point for the evaluation of configuration-mixing corrections to the magnetic moment.

The largest corrections to odd-A magnetic moments are due to the presence of certain seniority-3 components in the wave function. The magnetic-moment operator is a one-body operator which cannot change the orbital angular momentum of a nucleon. Seniority-3 components in the wave function can thus generate corrections to the magnetic moment (through nondiagonal matrix elements of the magnetic-moment operator with the seniority-1 components of the wave function) only when they differ from the seniority-1 components by the promotion of a single nucleon from one member of a spin-orbit doublet to the other. To the extent that odd-A antimony wave functions are predominantly of seniority 1 we are justified in evaluating these corrections with first-order perturbation theory. Details regarding these corrections can be found elsewhere.[2,13,14]

For odd-A antimony isotopes there are two types of first-order corrections. They may be written formally as

$$\delta\mu_{\mathrm{I}} = -2\sum_{J_p}\langle jj_1^{\,p_1}(0)|\vec{\mu}|j^2(J_p)j_1^{\,p_1-1}(j_1)\rangle\langle j^2(J_p)j_1^{\,p_1-1}(j_1)|\sum_{i<k}V_{ik}|jj_1^{\,p_1}(0)\rangle/|\Delta E|\,,$$

$$\delta\mu_{\mathrm{II}} = -2\langle j[j_1^{\,n_1}(0)j_2^{\,n_2}(0)]|\vec{\mu}|j\{[j_1^{\,n_1-1}(j_1)j_2^{\,n_2+1}(j_2)](1)\}\rangle\langle j\{[j_1^{\,n_1-1}(j_1)j_2^{\,n_2+1}(j_2)](1)\}|\sum_{i<k}V_{ik}|j \times [j_1^{\,n_1}(0)j_2^{\,n_2}(0)]\rangle/|\Delta E|\,,$$

where the energy denominator ΔE includes the single-particle energies and the interactions within levels, but does not include interactions between different levels. In $\delta\mu_{\mathrm{II}}$ the levels j_1 and j_2 are the two members of a spin-orbit doublet containing either neutrons or protons. By the application of well-known techniques, these formulas can be expressed in terms of one-particle matrix elements of the magnetic-moment operator and two-particle matrix elements of the nucleon-nucleon interaction[2]:

TABLE VII. Comparison of calculated and experimental values for magnetic moments of odd-A antimony isotopes. The moments are given in nuclear magnetons.

Isotope	$I(\pi)$	μ_{Schmidt}	$\delta\mu_{\mathrm{I}}+\delta\mu_{\mathrm{II}}$	$\delta\mu_{\vec{\mathrm{I}}\cdot\vec{\mathrm{s}}}$	$\delta\mu_{\mathrm{quench}}$	μ_{calc}	μ_{exp}
Sb^{113}	5/2(+)	+4.79	−0.91	−0.21	+0.24	+3.91	...
Sb^{115}	5/2(+)	+4.79	−0.91	−0.21	+0.24	+3.91	+3.46[a]
Sb^{117}	5/2(+)	+4.79	−0.91	−0.21	+0.24	+3.91	+2.67[a]
Sb^{119}	5/2(+)	+4.79	−0.88	−0.21	+0.24	+3.94	+3.45[a]
Sb^{121}	5/2(+)	+4.79	−0.86	−0.21	+0.24	+3.96	+3.36[b]
	7/2(+)	+1.72	+0.96	+0.22	−0.18	+2.72	+2.35[c]
Sb^{123}	7/2(+)	+1.72	+0.94	+0.22	−0.18	+2.70	+2.55[b]
	5/2(+)	+4.79	−0.84	−0.21	+0.24	+3.98	...
Sb^{125}	7/2(+)	+1.72	+0.90	+0.22	−0.18	+2.66	+2.62(6)[d]

[a] Present work.
[b] Reference 11,
[c] S. L. Ruby and G. M. Kalvius, Bull. Am. Phys. Soc. 12, 418 (1967).
[d] J. A. Barclay, W. D. Brewer, E. Matthias, and D. A. Shirley, University of California, Lawrence Radiation Laboratory Report No. UCRL-17716, 1967 (unpublished).

$$\delta\mu_{\mathrm{I}} = +2\begin{pmatrix} j & 1 & j \\ -j & 0 & j \end{pmatrix}\left[\frac{p_1}{2j_1+1}\right]\langle j_1 \| \mu \| j\rangle \sum_{\substack{J_p \neq 0 \\ \text{even}}} \frac{2(2J_p+1)}{|\Delta E|} \begin{Bmatrix} j_1 & j & J_p \\ j & j & 1 \end{Bmatrix} \langle j_1 j (J_p) | V_{12} | jj(J_p)\rangle ,$$

$$\delta\mu_{\mathrm{II}} = -2\begin{pmatrix} j & 1 & j \\ -j & 0 & j \end{pmatrix}\left[\frac{n_1}{2j_1+1}\right]\left[\frac{2j_2+1-n_2}{2j_2+1}\right]\langle j_1 \| \mu \| j_2\rangle \sum_K (-1)^{K+1+j_2-j}\frac{(2K+1)}{|\Delta E|}\begin{Bmatrix} j_1 & j_2 & 1 \\ j & j & K \end{Bmatrix}\langle j_1 j(K)|V_{12}|j_2 j(K)\rangle$$

For the reduced matrix element $\langle j_1 \| \mu \| j_2\rangle$ we have

$$\langle j_1 \| \mu \| j_2 \rangle = (-1)^{l+\frac{1}{2}+j_2}(g_l - g_s)[2l(l+1)/(2l+1)]^{\frac{1}{2}}.$$

In order to apply these formulas, we must choose matrix elements of the nucleon-nucleon interaction and determine the specific nature of the seniority-0 neutron wave function. We have employed matrix elements of the Hamada-Johnston potential as calculated by Kuo.[15] These matrix elements were evaluated with harmonic oscillator wave functions. They include the bare interaction and contributions from interactions involving one-particle one-hole intermediate states. Details are given for the calculation of such matrix elements in Ref. 16. No attempt has been made to renormalize the magnetic moment operator in the above moment corrections, and free-space values of $(g_l - g_s)$ have been used throughout.

It would be possible to obtain the seniority-0 neutron wave function by using the Hamada-Johnston matrix elements, but since small errors in these matrix elements could have a significant effect on the wave function, we favor an empirical approach. We approximate the wave function for odd-A Sb^A as a single proton coupled to the spin-0, seniority-0 ground state of the even = even isotope Sn^{A-1}. The neutron configuration of Sn^{A-1} is taken from the experimentally determined fractional occupancies of the five-neutron levels between $N = 50$ and $N = 82$.[17] These data indicate that the $2d_{5/2}$ and $1g_{7/2}$ levels are essentially filled in the ground states of tin isotopes of even mass number. To the extent that this tin wave function is of seniority 0, it may be described as a linear combination of the states which can be constructed from $(N-64)/2$ pairs of neutrons in the $2d_{3/2}$, $3s_{1/2}$, and $1h_{11/2}$ single-particle levels. Making these approximations, we find that those seniority-3 configurations which have a nonvanishing matrix element of the magnetic-moment operator with a given component of the unperturbed seniority-1 antimony wave function, have nonvanishing matrix elements of the two-body interactions with only that same seniority-1 component. In the expressions for first-order configuration-mixing moment corrections we can thus replace the terms $n_i/(2j_i+1)$ with the experimentally determined fractional occupancies of the neutron levels j_i, achieving a considerable simplification in the calculation.

It is necessary to know the spin-orbit doublet splitting in order to evaluate the energy denominators in the expressions for $\delta\mu_{\mathrm{I}}$ and $\delta\mu_{\mathrm{II}}$. The $2d$-neutron doublet-splitting is taken from the data of Schneid *et al.*[17] The $1g$ neutron doublet splitting is assumed to be 6.1 MeV and the $1h$ neutron splitting is assumed to be 6.7 MeV in agreement with Cohen.[18] Proton-doublet splittings are assumed to be the same as the corresponding neutron splittings.

There are several other corrections which should be applied to odd-A magnetic moments. Mayer and Jensen[19] first suggested that the presence of a central spin-orbit force (such as that needed to account for the observed shell-model doublet separations) gives rise to a correction to the magnetic moment of a proton in the nucleus. The nature of this correction is determined by the requirement of gauge invariance. The above authors estimate the magnitude of this contribution (in μ_N) to be

$$\delta\mu_{\vec{l}\cdot\vec{s}} \sim \mp 0.25(2j_p+1)/(2j_p+2)$$

for a proton in the state $j_p = l_p \pm 1/2$. We include this correction in the odd-A moment calculations.

Because of the exclusion principle, many of the virtual meson states which contribute to the anomalous moment of the free nucleon are forbidden for a nucleon in a nucleus. Drell and Walecka[20] and Nyman[21] have estimated this effect to lowest order. Nyman has also calculated the moment contributions resulting from meson exchange in excited states with two particles outside a one-hole core using the Hamada-Johnston potential. He estimates a 14% increase in anomalous moments, independent of nuclear mass. This correction has been applied.

The calculated odd-A antimony magnetic moments are listed in Table VII. These values include the effects of first-order configuration mixing, the spin-orbit force correction, and quenching corrections. The average deviation of $0.5\mu_N$ from the measured moments is satisfactory and represents a significant improvement over the mean deviation of $1.25\mu_N$ which results from the use of Schmidt moments. The calculation does not reproduce differences between the moments of nuclei with the same proton configuration.

B. Odd-Odd Magnetic Moments

In the simplest shell-model picture of an odd-odd nucleus, an unpaired proton in the state j_p and an unpaired neutron in the state j_n are coupled to spin I. All other nucleons are assumed to couple to spin 0. The magnetic moment of such a configuration, analogous to the Schmidt moment for odd-A nuclei, is given by the Landé formula:

$$\mu = (\mu_p/j_p)[I(I+1)+j_p(j_p+1)-j_n(j_n+1)/2(I+1)] + (\mu_n/j_n)[I(I+1)+j_n(j_n+1)-j_p(j_p+1)/2(I+1)].$$

We could proceed as in the previous section, evaluating the corrections to this moment; however, Caine[22] has shown that, to first-order, we can determine the configuration-mixing corrections to an odd-odd moment by replacing the Schmidt values of μ_p and μ_n in the above expression with the empirical moments of the states j_p and j_n as given by the measured moments of the odd-A nuclei $(Z, N-1)$ and $(Z-1, N)$ and by including certain uniquely odd-odd corrections. These corrections correspond to a change of the spin of the systems $(Z, N-1)$ and $(Z-1, N)$ and thus cannot be taken empirically. The use of empirical moments has the advantage of providing an empirical estimate of the quenching, spin-orbit, and exchange contributions to the moment.

The unique odd-odd configuration-mixing corrections are of two types which can be written formally as[2]

$$\Delta\mu_{p\text{-}\mathrm{I}} = -2 \sum_{J_p, J_1} \langle j_1^{2j_1+1}(0) j_p^{\,p}(j_p) j_n^{\,n}(j_n) I \,|\, \vec{\mu} \,|\, [j_1^{2j_1}(j_1) j_p^{\,p+1}(J_p)](J_1) j_n^{\,n}(j_n) I \rangle$$

$$\times \langle [j_1^{2j_1}(j_1) j_p^{\,p+1}(J_p)](J_1) j_n^{\,n}(j_n) I \,|\, \sum_{i<k} V_{ik} \,|\, j_1^{2j_1+1}(0) j_p^{\,p}(j_p) j_n^{\,n}(j_n) I \rangle / |\Delta E|$$

$$\Delta\mu_{p\text{-}\mathrm{II}} = -2 \sum_{J_p, J_1} \langle j_p^{\,p}(j_p) j_n^{\,n}(j_n) I \,|\, \vec{\mu} \,|\, [j_p^{\,p-1}(J_p) j_1](J_1) j_n^{\,n}(j_n) I \rangle$$

$$\times \langle [j_p^{\,p-1}(J_p) j_1](J_1) j_n^{\,n}(j_n) I \,|\, \sum_{i<k} V_{ik} \,|\, j_p^{\,p}(j_p) j_n^{\,n}(j_n) I \rangle / |\Delta E|.$$

An expression for these corrections in terms of one-particle matrix elements of the magnetic-moment operator and two-particle matrix elements of the nucleon-nucleon interaction is quite complicated. In the special case of a δ-function interaction $V(\vec{r}_{12}) = V_0\delta(\vec{r}_{12}) + \vec{\sigma}_1 \cdot \vec{\sigma}_2 V_1 \delta(\vec{r}_{12})$ these corrections assume the simpler forms

$$\Delta\mu_{p\text{-}\mathrm{I}} = -\{[2(j_p \mp j_n + I + 2)(j_p + j_n - I + 1)(j_p - j_n + I + 1)(j_n - j_p + I)]^{1/2} / 2(I+1)\}[(g_s - g_l)_p/(2l_p+1)]$$

$$\times \{[(2j_n + 1 - 2n)/(2j_n - 1)] \langle j_1 j_n I \,|\, V_0 \delta(r_1 - r_2) \,|\, j_p j_n I \rangle + [(2j_p + 1 - 2p)/(2j_p - 1)]$$

$$\times \langle j_1 j_n I \,|\, V_1 \vec{\sigma}_1 \cdot \vec{\sigma}_2 \delta(r_1 - r_2) \,|\, j_p j_n I \rangle\} / |\Delta E|,$$

$$\Delta\mu_{p-\mathrm{II}} = -2\{[(j_p + j_n + I + 1)(j_p + j_n - I)(j_p - j_n + I)(j_n - j_p + I + 1)]^{\frac{1}{2}} / 2(I+1)\}[(g_s - g_l)_p/(2l_p+1)]$$

$$\times [(2j_n + 1 - 2n)/(2j_n - 1)] \langle j_1 j_n I \,|\, V_0 \delta(r_1 - r_2) \,|\, j_p j_n 1 \rangle + [(2j_p + 1 - 2p)/(2j_p - 1)] \langle j_1 j_n I \,|\, V_1 \vec{\sigma}_1 \cdot \vec{\sigma}_2 \delta(r_1 - r_2) \,|\, j_p j_n I \rangle\} / |\Delta E|,$$

where $\delta(r_1 - r_2)$ includes only the radial δ function.

In the calculation of odd-odd moment corrections, we employ a δ-function interaction with $V_1/V_0 = 0.091$ to correspond with the normal ratio between the strengths of the singlet and triplet forces. A value of -3.0 MeV for V_0 provides the best fit of these δ-function matrix elements to the more realistic Hamada-Johnston matrix elements described above.

Most of the necessary empirical odd-proton moments are available (see Table VII). This is not the case for the odd-neutron moments. We therefore make use of other nearby empirical neutron-moments, which are presumed to provide an adequate approximation to the desired empirical values. The empirical odd-neutron moments used in this calculation are given in Table VIII, with the nuclei from which the values were obtained.

This calculation again requires knowledge of the fractional occupancies of the neutron levels. Experi-

mental values are available only for the ground states of the odd-mass tin isotopes, which do not always have the desired spin. We again assume that the $2d_{5/2}$ and $1g_{7/2}$ levels are essentially filled and that we need only distribute $(N-65)/2$ pairs of neutrons among the states $2d_{3/2}$, $3s_{1/2}$, and $1h_{11/2}$. The odd neutron is always assumed to be in the level j_n. A calculation with Hamada-Johnston matrix elements suggests that the fractional occupancies for the lowest-lying seniority-1 states of spin and parity $\frac{3}{2}^+$, $\frac{1}{2}^+$, and $\frac{1}{2}^-$ are approximately equal. The experimentally-determined fractional occupancies for the ground states of odd-mass Sn^{A-1} have thus been used in the above expressions for the moment corrections in odd-odd Sb^A, independent of the spin of Sn^{A-1}.

The caluclated odd-odd antimony magnetic moments are compared with the experimental values in Table IX. The calculations have been made for the odd-particle locations which were the most favorable energetically. Since a better approximation to the odd-odd antimony wave functions would involve mixtures of several odd-particle locations of the same seniority, we should not expect our treatment of the odd-odd isotopes to give agreement as good as that obtained in the odd-A moment calculations. The reliability of this calculation is also limited by the unavailability of the required empirical moments, the approximations involved in estimating the fractional occupancy of neutron levels, and our restriction to a δ-function interaction. It is thus not surprising that the average deviation of $0.6\,\mu_N$ indicates no improvement over the moment estimates obtained from the uncorrected Landé formula using Schmidt-moments.

ACKNOWLEDGMENTS

We would like to express our deep appreciation to Professor D. R. Hamilton and Professor E. A. Phillips of Princeton University, and Professor O. Ames of the State University of New York at Stony Brook for their skillful guidance and expert advice at all stages of this work. We also wish to thank Professor T. T. S. Kuo of Princeton University for the use of his matrix elements and for the benefit of many helpful discussions.

TABLE VIII. Neutron g factors.

Neutron state	g_{Schmidt}	$g_{\text{empirical}}$	Reference isotopes (See Ref. 11.)
$3s_{1/2}$	-3.82	-1.98 (6)	$Sn^{115, 117, 119}$
$2d_{3/2}$	+0.76	+0.47 (4)	Sn^{119m}
$2d_{5/2}$	-0.76	-0.29 (3)	$Cd^{107, 109}$
$1h_{11/2}$	-0.35	-0.19 (2)	$Cd^{113m, 115m}$

TABLE IX. Comparison of calculated and experimental values for magnetic moments of odd-odd antimony isotopes. The moments are given in μ_N. The spin and parity assignments (I, π) in parentheses are uncertain.

Isotope	$t_{1/2}$	Proton state	Neutron state	I, π	μ_{Schmidt}	μ_{emp}	$\Delta\mu$	μ_{calc} [a]	μ_{exp}
Sb^{116}	15.5 min	$d_{5/2}$	$s_{1/2}$	3, + [b]	+2.89	+2.47	+0.00	+2.47	• • •
		$d_{5/2}$	$d_{3/2}$		+4.73	+3.35	−0.18	+3.17	
Sb^{116m}	60 min	$d_{5/2}$	$h_{11/2}$	(8, −)	+2.88	+2.40	+0.00	+2.40	• • •
Sb^{118}	3.5 min	$d_{5/2}$	$d_{3/2}$	1, +	+2.80	+1.51	+0.22	+1.73	± 2.46(7) [c]
Sb^{118m}	5.1 h	$d_{5/2}$	$h_{11/2}$	(8, −)	+2.88	+1.62	+0.00	+1.62	• • •
Sb^{120}	16 min	$d_{5/2}$	$d_{3/2}$	1, +	+2.80	+2.06	+0.04	+2.10	± 2.3(2) [c]
Sb^{120}	5.8 days	$d_{5/2}$	$h_{11/2}$	(8, −)	+2.88	+2.40	+0.00	+2.40	• • •
Sb^{122}	2.8 days	$g_{7/2}$	$h_{11/2}$	2, −	−2.64	−2.39	−0.08	−2.47	−1.90 [d]
Sb^{122m}	4.2 min	$g_{7/2}$	$h_{11/2}$	(7, −) [d]	−0.54	+0.61	−0.10	+0.51	• • •
Sb^{124}	60 days	$g_{7/2}$	$h_{11/2}$	3, −	−1.88	−1.48	−0.43	−1.91	±1.26(7) [e]

[a] $\mu_{\text{calc}} = \mu_{\text{emp}} + \Delta\mu$.
[b] G. J. Garrett, private communication.
[c] Present work.
[d] P. C. B. Fernando, G. K. Rochester, and K. F. Smith, Phil. Mag. 5, 1309 (1960).
[e] T. F. Knott, H. R. Andrews, B. Greenebaum, and F. M. Pipkin, Phys. Rev. 170, 1051 (1968).

†This work was supported by the U. S. Atomic Energy Commission and the Higgins Scientific Trust Fund and made use of the computer facilities supported in part by the National Science Foundation Grant NSF-GP-579.

* Present address: Department of Physics, State University of New York, Stony Brook, New York.

‡ Present address: Department of Physics, Allegheny College, Meadville, Pennsylvania.

§ Present address: Department of Chemistry and Physics, State College of Massachusetts at Worcester, Worcester, Massachusetts.

[1]R. J. Blin-Stoyle and M. A. Perks, Proc. Phys. Soc. (London) A67, 885 (1954).

[2]H. Noya, A. Arima, and H. Horie, Progr. Theoret. Phys. (Kyoto) 8, 33 (1958).

[3]N. F. Ramsey, Molecular Beams (Oxford University Press, London, 1956).

[4]H. Kopfermann, Nuclear Moments (Academic Press, Inc., New York, 1958).

[5]A. M. Bernstein, R. A. Haberstroh, D. R. Hamilton, M. Posner, and J. L. Snider, Phys. Rev. 136, B27 (1964).

[6]O. Ames, E. A. Phillips, and S. S. Glickstein, Phys. Rev. 137, B1157 (1965).

[7]Unless otherwise indicated, statements regarding half lives and decay schemes of tin and antimony isotopes are based on Nuclear Data Sheets, compiled by K. Way *et al.* (National Academy of Sciences–National Research Council, Washington, D.C., 1963), NRC 60-2-89 through NRC 61-2-121.

[8]J. W. Mihelich and R. D. Hill, Phys. Rev. 79, 781 (1950).

[9]The hfs data were analyzed using the computer program HYPERFINE-4A, Princeton's version of the Berkeley hyperfine-structure program described by V. J. Ehlers and H. A. Shugart, Phys. Rev. 127, 529 (1962).

[10]P. C. B. Fernando, G. K. Rochester, I. J. Spalding, and K. F. Smith, Phil. Mag. 5, 1291 (1960).

[11]Appendix I to Nuclear Data Sheets, compiled by G. H. Fuller and V. W. Cohen (U. S. Government Printing Office, National Academy of Sciences – National Research Council, Washington, D. C., 1965).

[12]K. Murakawa, Phys. Rev. 93, 1232 (1954).

[13]R. J. Blin-Stoyle, Rev. Mod. Phys. 28, 75 (1956).

[14]H. A. Mavromatis, Princeton University Technical Report No. PUC-937-193 (unpublished).

[15]T. T. S. Kuo (Princeton University), private communication.

[16]T. T. S. Kuo, Nucl. Phys. A90, 199 (1967).

[17]E. J. Schneid, A. Prakash, and B. L. Cohen, Phys. Rev. 156, 1316 (1967).

[18]B. L. Cohen, Phys. Rev. 130, 227 (1963).

[19]J. H. D. Jensen and M. Goeppert-Mayer, Phys. Rev. 85, 1040 (1952).

[20]S. D. Drell and J. D. Walecka, Phys. Rev. 120, 1069 (1960).

[21]E. M. Nyman, Nucl. Phys. B1, 535 (1967).

[22]C. A. Caine, Proc. Phys. Soc. (London) A69, 635 (1956).